Experimental study of the impact of large-scale wind farms on land–atmosphere exchanges

Wei Zhang[1]**, Corey D Markfort**[1] **and Fernando Porté-Agel**[2]

[1] Saint Anthony Falls Laboratory, Department of Civil Engineering, University of Minnesota,
Minneapolis, MN 55414, USA
[2] Wind Engineering and Renewable Energy Laboratory (WIRE), École Polytechnique Fédérale de
Lausanne (EPFL), EPFL-ENAC-IIE-WIRE, CH-1015 Lausanne, Switzerland

E-mail: fernando.porte-agel@epfl.ch

Abstract
Large-scale wind farms, covering a significant portion of the land and ocean surface, may affect the
transport of momentum, heat, mass and moisture between the atmosphere and the land locally and
globally. To understand the wind-farm–atmosphere interaction, we conducted wind-tunnel experiments to
study the surface scalar (heat) flux using model wind farms, consisting of more than ten rows of wind
turbines—having typical streamwise and spanwise spacings of five and four rotor diameters—in a neutral
boundary layer with a heated surface. The spatial distribution of the surface heat flux was mapped with an
array of surface heat flux sensors within the quasi-developed regime of the wind-farm flow. Although the
overall surface heat flux change produced by the wind farms was found to be small, with a net reduction of
4% for a staggered wind farm and nearly zero change for an aligned wind farm, the highly heterogeneous
spatial distribution of the surface heat flux, dependent on the wind-farm layout, was significant. The
difference between the minimum and maximum surface heat fluxes could be up to 12% and 7% in aligned
and staggered wind farms, respectively. This finding is important for planning intensive agriculture
practice and optimizing farm land use strategy regarding wind energy project development. The
well-controlled wind-tunnel experiments presented in this study also provide a first comprehensive dataset
on turbulent flow and scalar transport in wind farms, which can be further used to develop and validate
new parameterizations of surface scalar fluxes in numerical models.

Keywords: surface heat flux, turbulence, wind-farm–atmosphere interaction, wind-tunnel experiment

1. Introduction

As global wind power capacity is growing exponentially, it is
foreseen that many more large-scale wind farms will be built
onshore and offshore. It is of great interest to understand how
they may affect the transport of momentum, heat, moisture
and trace gases (e.g. CO_2) between the land surface and the
atmosphere, and possible subsequent environmental impacts
in terms of long-term sustainability of wind power (Baidya
Roy 2011). Some of the best wind resources in the US, for
example, are over farmland, especially in the central plains
(Gunturu and Schlosser 2012). In these regions, near-surface
momentum, heat and moisture transport can be very important
because changes in surface meteorological conditions (e.g.,
the near-surface wind speed, daily maximum and minimum
temperatures, surface sensible and latent heat flux) affected
by wind farms, may impact local agricultural practices. In
some cases, the impact may be beneficial. For example, a
field experimental campaign on wind-turbine wake effects

on crops in central Iowa found that the wind turbine cools the near-surface air in the summer, which helps crops thrive (crop/wind-energy experiment or CWEX, see Rajewski *et al* 2012). However, potential drying and increased irrigation requirement may not be a favorable effect.

Modeling studies of the influence of utility-scale wind farms on regional and global climate have shown that the impacts may be substantial (Ivanova and Nadyozhina 2000, Baidya Roy *et al* 2004, Keith *et al* 2004, Baidya Roy and Traiteur 2010, Barrie and Kirk-Davidoff 2010, Baidya Roy 2011, Wang and Prinn 2011, Fitch *et al* 2012, Zhou *et al* 2012). For instance, Baidya Roy (2011) found that wind farms significantly affected near-surface air temperature and humidity as well as surface sensible and latent heat fluxes. The signs of the impacts (i.e., increase or decrease), are reported to depend on static stability and total water mixing ratio lapse rates of the atmosphere. Recent high-resolution large-eddy simulation (LES) studies are able to resolve detailed fluid dynamics and heat transport within and over wind farms as well as near the land surface (Calaf *et al* 2010, 2011, Lu and Porté-Agel 2011, Porté-Agel *et al* 2011, Wu and Porté-Agel 2011). Lu and Porté-Agel (2011) reported that the surface momentum and heat fluxes in a very large wind farm underwent substantial reduction of more than 30% and 15% respectively, relative to that of the stable boundary-layer flow without wind turbines. In contrast, Calaf *et al* (2011) found surface heat flux increased by 10%–15% and a reduction of the momentum flux, from their LES study of wind-farm flows subjected to a neutral boundary layer with temperature as a passive scalar. It is not clear what key factors lead to the different results of the surface heat flux change.

So far most studies on near-surface temperature and fluxes altered by large-scale wind farms have been carried out by numerical simulations. In fact, rarely are these studies validated against observational evidence (Baidya Roy and Traiteur 2010). The computational results are dependent on the accuracy of the models employed and the realism of the methods applied to parameterize wind turbines (e.g., Barrie and Kirk-Davidoff 2010, Wang and Prinn 2010). In particular, the validity of representing the impacts of wind-turbine arrays on momentum transport by the widely applied added roughness length models needs further study, evidenced by Markfort *et al* (2012). Therefore, new observations in the field and laboratory are in high demand to advance our understanding of turbulent wakes and scalar transport in wind farms and for numerical model development.

There are few laboratory studies or field observations on land–atmospheric scalar or heat transport in wind farms. Though field observation is generally preferred, point-based measurements of heat, water vapor and CO_2 fluxes are very challenging to interpret due to flow non-stationarities as well as turbulence heterogeneity around turbines. Wind-tunnel simulations have proved to be very valuable to study the turbulent wake characteristics and momentum/heat transport in scaled-down wind farms (e.g., Cal *et al* 2010, Chamorro and Porté-Agel 2011, Chamorro *et al* 2011, Markfort *et al* 2012). High spatial and temporal resolution data taken under well-controlled conditions not only provide the full picture of turbulent flow and flux characteristics but contain sufficient details to validate numerical models.

The goal of this study is to acquire direct measurements of the spatial distribution of the surface heat flux altered by large-scale wind farms, as well as the turbulent flow and flux characteristics near the surface in a thermally controlled wind tunnel. This work will advance our understanding of turbulent transport and surface scalar (heat) flux within a large-scale wind farm, provide comprehensive datasets for validating numerical models and improve planning and interpretation of field observations.

2. Facilities, models and measurements

Experiments were carried out in the closed-loop thermally controlled boundary-layer wind tunnel at the Saint Anthony Falls Laboratory, University of Minnesota. The main test section for boundary-layer flow studies has a length of 16 m and a cross-section of 1.7×1.7 m^2. The facility is able to achieve desired thermal stratification conditions by controlling the air and the floor temperature independently in the range of $5\,°C$–$80\,°C \pm 0.25\,°C$. To generate a deep turbulent boundary layer with the depth (δ) of 0.5 m, a tripping mechanism (40-mm picket fence) was used at the entrance of the test section. Primary characteristics of the simulated turbulent boundary layer with a surface heat source are summarized in table 1. With the freestream wind speed (U_∞) set at 3.2 ms^{-1}, the resulting bulk Richardson number Ri_b is -0.09 and the Obukhov length L is about 0.4 m. Though the floor was heated to $72\,°C$, the enhanced buoyancy effect is negligible due to the shear and additional turbulence generated by wakes within the wind farms. It follows that the heat source at the surface does not affect the dynamics of the flow within the wind farms, thus heat is treated as a passive scalar (Markfort *et al* 2012).

The model wind farms were composed of miniature model wind turbines, which were employed in previous wind-turbine wake studies (e.g., Chamorro *et al* 2011, Markfort *et al* 2012, Zhang *et al* 2012a, Zhang *et al* 2012b). The rotor diameter d is 0.128 m and the hub height is 0.104 m, with the bottom tip of the turbine at a height of 0.04 m and the top tip at 0.168 m high. The rotor swept area of the turbines is within the lowest 1/3 of the turbulent boundary layer, ensuring geometric similarity with field-scale wind farms. Two idealized wind-farm layouts, perfectly aligned and staggered wind farms were studied, as illustrated in figure 1. In both wind farms, the rotor plane of each wind turbine is perpendicular to the main direction of the flow. The turbines rotate in a counter-clockwise manner, inducing the clockwise rotation of the wake when looking downwind. The aligned farm consists of a wind-turbine array of 12 rows and 3 columns, with a typical streamwise spacing of 5d and the spanwise spacing of 4d. The staggered wind farm has the same arrangement in the odd-numbered rows as the aligned farm, while two turbines in the even-numbered rows are shifted by 2d in the spanwise direction. It is noted that the top-tip height of a turbine or the wind-farm height $Z_H (=1.3d)$ was found to be a key length scale to characterize the turbulent

Table 1. Characteristics of the turbulent boundary layer with a surface heat source.

Floor θ_s (°C)	Air θ_0 (°C)	Roughness z_0 (mm)	Friction vel. u_* (m s^{-1})	Re$_\delta$ (= $U_\infty \delta / \nu$)	Ri_b	δ/L
72	12	0.08	0.12	1×10^5	−0.09	−1.25

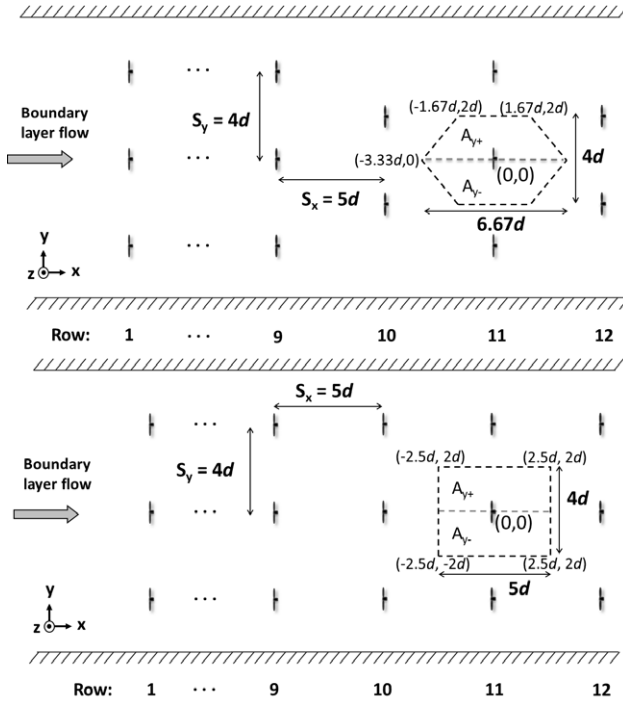**Figure 1.** Schematic diagram of wind-turbine array arrangement in the staggered (upper) and aligned (bottom) wind farms.

Figure 2. Schematic diagram of the energy balance analysis in a control volume for the fully developed wind-farm flow regime.

flow and thus being used to normalize the height above the surface (Markfort *et al* 2012).

The right-handed Cartesian coordinate system is defined in figures 1 and 2. Similar coordinate definition was used in Calaf *et al* (2011), Markfort *et al* (2012) and Wu and Porté-Agel (2012). As the spatial distribution and change of surface heat flux in an effective unit area (*A*) is of particular interest, we set the origin at the center of *A*, where the target turbine is located. It is important to note that the distributed wind-turbine density is the same for both wind-farm layouts, with *A* of $20d^2$ per wind turbine. For the convenience of discussion, *A* is further divided into specific sub-areas: the near-wake region A_{NW} ($x/d = [0, 1]$, $y/d = [−0.22, 0.22]$), the downwelling side of the wake A_{y-} ($y/d = [−2, 0]$) and the upwelling side of the wake A_{y+} ($y/d = [0, 2]$). The limit of x/d varies between −3.33 and 3.33 depending on y/d in A_{y-} and A_{y+} for the staggered farm, while it is constant ($=[−2.5, 2.5]$) in A_{y-} and A_{y+} for the aligned farm.

Measurements of the surface heat flux were made using flat-plate type heat flux sensors (Captec, Inc.). The thin-foil heat flux sensor consists of a thermoelectric panel laminated between flexible heterogeneous plastic layers. Each heat flux sensor is 0.01 m by 0.01 m, with a thickness of 0.4 mm to minimize flow disturbance caused by mounting them on
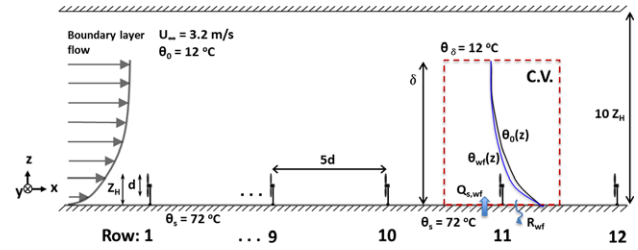
the surface. A silicone-based heat sink compound was used to ensure good contact between the sensor and the surface. The heat transfer sensitivity of the sensor is 0.6 V W^{-1} m^2 and the response time is 0.3 s. Heat flux was calculated by dividing the voltage output, which is proportional to the heat flux through the sensor, by the sensor sensitivity. An array of 19 sensors was mounted to cover the spanwise distance from $y/d = [−2, 2]$, with an even spacing (Δy) of $0.22d$. Measurements in the streamwise direction were conducted by shifting the entire wind farms multiple times by $\Delta x = 0.5d$ to cover *A*. Data were recorded every 5 s for 20–30 min to ensure the convergence of measurements.

Once the spatial distribution of heat flux q_s (the surface heat flux at each measured node) is acquired, the overall surface heat flux Q_s is calculated by

$$Q_s = \frac{1}{A} \int q_s \, dA. \tag{1}$$

In addition, a high-frequency triple-wire (combination of a *x*-wire and a cold-wire) anemometer was used to measure vertical profiles of velocity and temperature at selected locations within the wind farm, to understand the vertical momentum and heat transport near the surface. Detailed measurements of the turbulent flow within the same wind farms can be found in Markfort *et al* (2012).

3. One-dimensional energy balance analysis

For a very large wind farm with a length approaching or exceeding the height of the atmospheric boundary layer on flat terrain by a factor of 10 or more, a fully developed flow regime may ultimately appear and wind-farm flows are expected to display an asymptotic behavior (Meneveau 2012). It means that horizontally averaged flow quantities can be assumed to vary only as a function of height above the surface. Here we estimate the surface heat flux change induced by such large-scale wind farms from the viewpoint of vertical energy balance. This one-dimensional (1D) approach will be applied to the wind-farm flow to understand the effects of

wind farms on surface heat flux, considering that the model wind farm employed in this study allows the flow to reach a quasi-developed state with minimal entrance and side-edge effects at the measurement location.

The change in the internal energy of a system (ΔE) is equal to the sum of the heat added to the system (the balance of various sources of fluxes, ΔQ) and the work (ΔW) done by or on the system. A control volume (C.V.) is defined for the fully developed flow regime, as shown in figure 2. The bottom is the ground surface with a fixed temperature $\theta_s = 72\,^\circ\text{C}$, and the top is at the thermal boundary-layer height (δ_θ) with $\theta_\delta = 12\,^\circ\text{C}$. The net heat flux is zero due to the negligible temperature gradient at the top of the control volume. Also, there is no net flux at the upwind and downwind boundaries between wind-turbine rows since the flow is at equilibrium. On the surface there is a heat source Q and heat loss from radiation R. Accordingly, the energy budget of the control volume for a unit time is written as follows:

$$\Delta E = \Delta Q + \Delta W \qquad (2)$$

in this case ΔW is negligible, and

$$\Delta Q = Q_{s,wf} - R_{wf} - (Q_{s0} - R_0), \qquad (3)$$

where subscripts '$_0$' and '$_{wf}$' indicate the boundary-layer flow case and the wind-farm case, respectively. R_0, R_{wf} are estimated to be less than 0.2% of the internal energy due to the fact that the wind-tunnel floor is a polished aluminum surface. It follows that

$$\Delta Q = Q_{s,wf} - Q_{s0} = \rho C_p \int_0^{\delta_\theta} (\theta_{wf}(z) - \theta_0(z))\, dz, \qquad (4)$$

where ρ and C_p are air density and specific heat capacity. This equation indicates that the change in surface heat flux can be approximated by the change in the internal energy of the flow due to the presence of the wind farms.

4. Results and discussion

Spatial distribution of the surface heat flux will be presented for both staggered and aligned wind farms, and representative vertical profiles of turbulent flow and fluxes averaged over several spanwise locations in the quasi-developed flow regime will be shown to aid interpretation of these results. As found by Markfort *et al* (2012) and Wu and Porté-Agel (2012), the lateral turbulent mixing within wind-turbine arrays is more efficient in the staggered layout than in the aligned layout. This suggests that spanwise-averaged vertical profiles would better represent the wind-farm flow characteristics for the staggered wind farm than the aligned farm case. Therefore we will focus on the staggered wind-farm case by examining both the surface heat flux distribution and vertical profiles of the turbulent flow and fluxes near the surface. Afterwards, we will present and discuss the surface heat flux distribution pattern induced by the aligned farm. Also, it should be noted that the net change in surface heat flux, affected by wind farms, is relative to that of the boundary-layer flow without a wind farm.
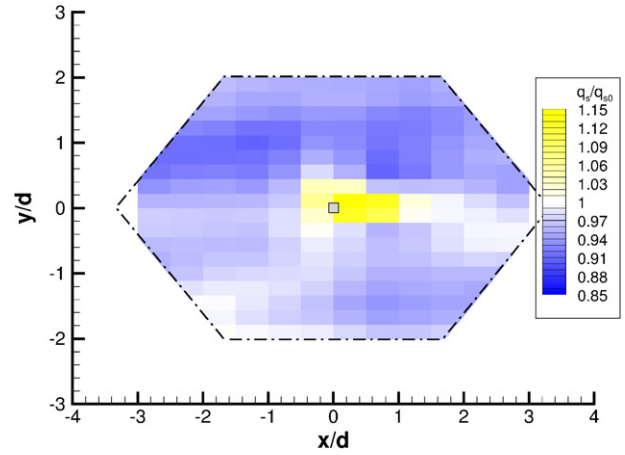

Figure 3. Spatial distribution of the mean surface heat flux in an unit area of the staggered farm.

4.1. Staggered wind-farm case

Spatial distribution of the surface heat flux (q_s) for a unit area in the staggered wind farm, relative to that of the boundary-layer flow without wind turbines (q_{s0}), is shown in figure 3. The surface heat flux is increased by about 24% in the sub-area A_{NW} near the base of the wind turbine due to the locally enhanced turbulent mixing. However, it should be noted that increased surface heat flux is limited to the region adjacent to the wind turbine. Outside this region, there is a relatively uniform distribution of decreased surface heat flux. As we shall see later, the pattern of surface heat flux distribution is associated with multiple-wake interaction near the surface in the wind farms. To quantify the net change of the surface heat flux, we summarize the surface heat flux aggregated in specific sub-areas in table 2. The data show an overall surface heat flux reduction of approximately 4% in the staggered wind farm compared to that of the boundary-layer flow, with higher values (by 3%) in sub-area A_{y-}, compared with those of A_{y+}. Results of the aligned farm case are also included here and will be discussed in section 4.2.

Figure 4(a) shows the spanwise-averaged kinematic heat flux ($\langle Q \rangle_y$) as a function of the height above the surface in the staggered farm case. One can see that the presence of the wind farm strongly affects the turbulent heat flux profile over and through the wind farm. The kinematic heat flux $\langle Q \rangle_y$ displays a higher magnitude than that in the boundary-layer flow without turbines, for $z > Z_H$. However, near the surface $\langle Q \rangle_y$ has a lower magnitude than Q_{s0}. This result is qualitatively consistent with the direct surface heat flux measurements. Calaf *et al* (2011) obtained near-linear scalar flux profiles, which is different from the complex behavior of the kinematic heat flux observed in measurements here. Their results indicate that the surface heat flux increased by 10%–15% in the presence of large-scale wind farms compared to the boundary-layer flow.

The change in near-surface air temperature induced by the presence of the wind farms is directly related to the surface heat flux change, and is also an important input of the 1D energy balance analysis. Figure 4(b) shows the comparison of
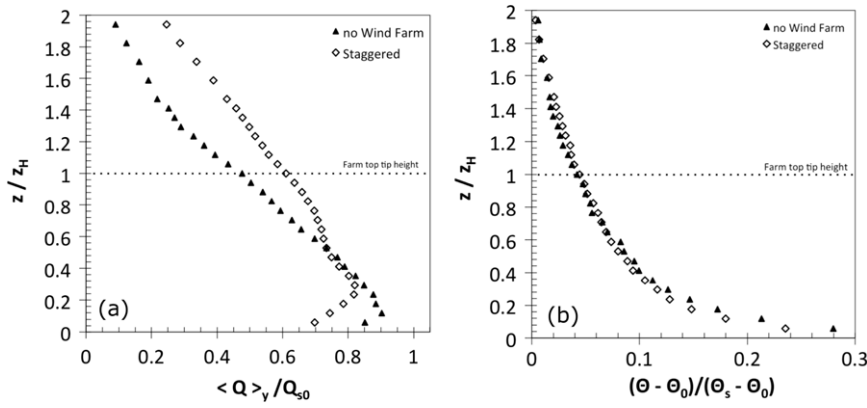
Figure 4. Vertical profiles of the spanwise-averaged kinematic heat flux and air temperature in the staggered farm, compared to that in the boundary-layer flow.

Table 2. Q_s/Q_{s0} in specific sub-areas of an effective unit area A in the staggered and aligned wind farms.

Wind-farm layout	A_{y-} $y/d = [-2, 0]$	A_{y+} $y/d = [0, 2]$	A_{NW} $y/d = [-0.22, 0.22], x/d = (0-1)$	Net effect
Staggered	0.972	0.943	1.240	0.962
Aligned	1.033	0.969	1.195	1.0

spanwise-averaged temperature profiles with and without the wind farm. Above Z_H, temperature profiles are quite similar for both cases. However, below $0.6Z_H$ the air temperature becomes less in the staggered wind farm than that in the boundary-layer flow. Approaching the surface, the decrease of air temperature in the wind farm becomes larger, about 3 °C at $z/Z_H = 0.06$. The reduced near-surface air temperature in the presence of the wind farm was also observed from previous field studies, though under statically unstable conditions. Using data collected from a meteorological field campaign at San Gorgonio, Baidya Roy and Traiteur (2010) found that the near-surface temperature in the wake downwind of the wind farms was reduced during the day. Furthermore, they related the increased near-surface air temperature gradient to more efficient heat transport from the ground surface to the atmosphere, and subsequently increased surface heat flux (Baidya Roy 2011). However, this reasoning assumes the flux–gradient relationship with a constant effective diffusivity of heat K_H $(= \frac{\overline{w'\theta'}}{\partial\theta/\partial z})$ for the flow near the surface with and without wind farms. In fact, in turbulent wind-farm flows K_H is highly dependent on the flow structure which is hard to know *a priori*. Indeed, as shown by Lu and Porté-Agel (2011), the vertical distribution of K_H is quite different in wind-farm cases compared to that in the boundary-layer flow. This is also supported by the measured turbulent Prandtl number (Pr_t) profiles (figure 17(b)) in our experiments, discussed in detail by Markfort *et al* (2012). Hence, it is problematic to assume a constant K_H near the surface and attribute the enhanced surface heat flux to increased near-surface temperature gradient.

Instead, if we consider the standard surface-layer scaling which assumes that the surface heat flux Q_s can be expressed as the product of a temperature scale θ_* and a velocity scale u_*, it has been found that the wind-farm induced change in

these two scales has an opposite trend. While the increased temperature gradients near the surface lead to an increase in θ_*, the decreased shear stress and reduced velocity result in a reduced u_* compared to the boundary-layer flow (Calaf *et al* 2011, Lu and Porté-Agel 2011, Markfort *et al* 2012). Whether the surface heat flux is altered by the presence of the wind farms, and if so, the sign (e.g., increase or decrease) is dependent on the competing effects of the magnitude of increased temperature scale θ_* and reduced velocity scale u_*. Unfortunately we are not able to determine the magnitude of u_* from the current data because there is no evident near-surface logarithmic layer detected within the wind farm.

Using the air temperature profile with the 1D energy budget analysis, we estimate that $Q_{s,wf}/Q_{so}$ is approximately 0.97 for the staggered wind-farm case. This result corroborates the overall reduction of the surface heat flux directly measured with surface heat flux sensors. The relationship (in equation (4)) clearly shows that the surface heat flux is reduced if the air temperature affected by the presence of the wind farms is lower than that of the boundary-layer case.

In addition, the turbulent linear correlation coefficient can be used as a measure of the overall efficiency of turbulent transfer mechanism in complex turbulent flows (Roth and Oke 1995). Specifically, $r_{w\theta} = \frac{\overline{w'\theta'}}{\sigma_w\sigma_\theta}$ is an indicator of the overall heat transfer efficiency. A value of unity means the efficiency of heat transfer is optimal. The variation of $r_{w\theta}$ with height in the staggered wind-farm case, in figure 5, shows the relative efficiency between the wind farm and the boundary-layer flows. Above Z_H the heat transfer efficiency $r_{w\theta}$ of the wind-farm case is comparable to that of the boundary-layer flow. Within the wind farm, however, $r_{w\theta}$ generally decreases with decreasing height above the surface. As approaching the surface, the heat transfer efficiency $r_{w\theta}$ of the staggered wind farm is about 70% of that of the boundary-layer flow.
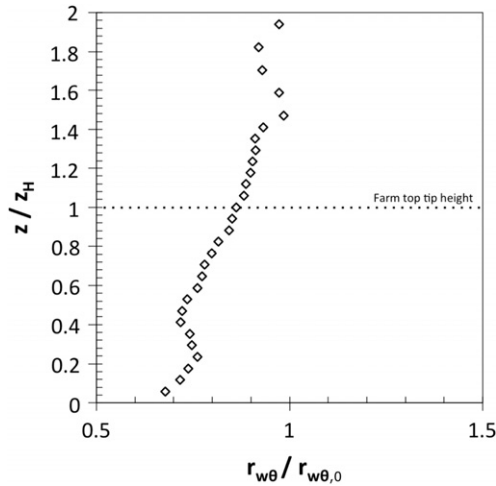
Figure 5. Vertical profile of the heat transfer efficiency in the staggered wind farm, compared to that of the boundary-layer flow.
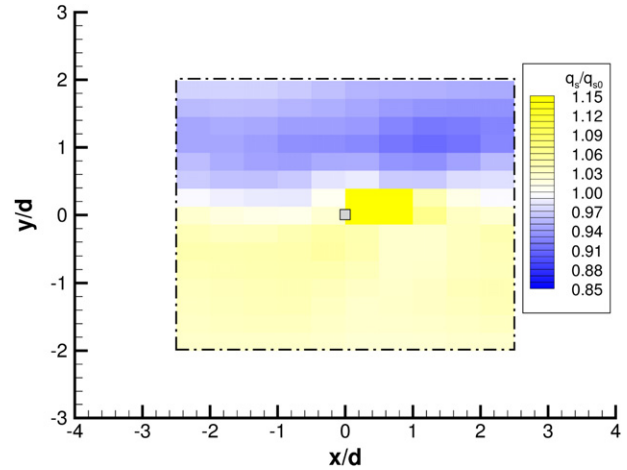

Figure 6. Spatial distribution of the mean surface heat flux in a unit area of the aligned farm.

This result indicates that the increased turbulence and heat transport above the wind farm do not necessarily translate into higher surface heat flux at the ground.

4.2. Aligned wind-farm case

Wind-farm configuration has been found to appreciably affect the momentum and heat transport within and above the wind farm (Markfort *et al* 2012). Here we present the surface heat flux distribution of an unit area in a perfectly aligned farm case (figure 6). Similar to the staggered wind-farm case, the surface heat flux is increased by about 20% near the base of the wind turbine in the sub-area A_{NW}. Outside this region, the surface heat flux displays an interesting pattern, very different from the relatively uniform distribution of reduced heat flux in the staggered wind farm. The change of the surface heat flux displays a distinct opposite trend on either side of the column of turbines, with increased heat flux in A_{y-} and reduced heat flux in A_{y+}. A similar magnitude of increased and decreased heat flux on the two sides yields a nearly zero net change in the surface heat flux (see table 2). To give an additional quantitative measure of the surface heat flux magnitude, the distribution of surface heat flux as a function of the spanwise location is shown for both wind farms in figure 7. The difference between the maximum and minimum surface heat flux is about 12% of Q_{s0} in the aligned wind farm and 7% of Q_{s0} (with the minimum being $0.92Q_{s0}$) in the staggered farm. The results indicate that the spatial distribution of surface heat flux is noticeably heterogeneous for both cases, though heat flux displays a relatively uniform distribution in the staggered wind farm.

Multiple-wake interaction and the wake boundary-layer flow interaction are the dominant mechanisms of momentum and heat transport in large-scale wind-farms (see Vermeer *et al* 2003, Frandsen *et al* 2006, Frandsen *et al* 2009). The spatial distribution of the surface scalar flux is particularly affected by the complicated wake interactions. The distinct regions of increased versus decreased surface heat flux, with
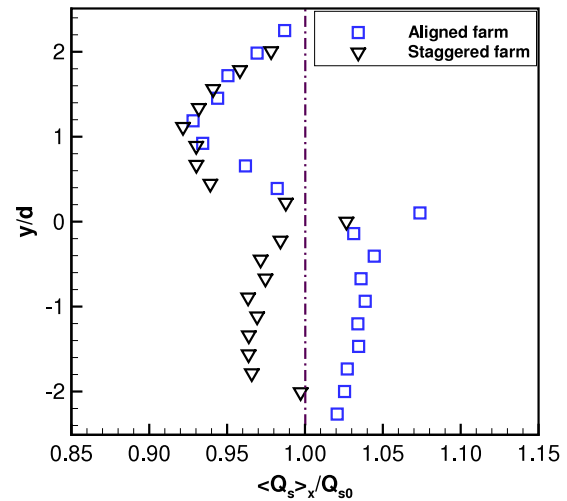

Figure 7. Surface heat flux integrated along the streamwise direction, as a function of the spanwise location in the aligned and staggered wind farms.

respect to the turbine column in the aligned farm case, are correlated with the wake evolution and wake rotation in the turbine array. Within large-scale wind farms, flow under the effects of multiple-wake interaction can be classified into several regimes (Frandsen *et al* 2006): the individual wake behind the first row of wind turbines (regime I); multiple wakes evolving from a single column of turbines (regime II); wake merging from neighboring turbine columns (regime III); and finally sufficiently mixed wake flow reaching a fully developed state. According to this division of the wake regimes, it is conjectured that the aligned farm case is subjected to an overlapping coherent wake column—formed primarily from the single column of turbines, i.e. regime III—rotating in a clockwise manner when looking downwind. Subsequently, increased surface heat flux occurs in A_{y-} as cooler air is brought from above to the surface, while reduced heat flux is observed for the region of A_{y+} as warmer air moves upwards away from the surface. The difference in air temperature profiles, measured on the two sides of the
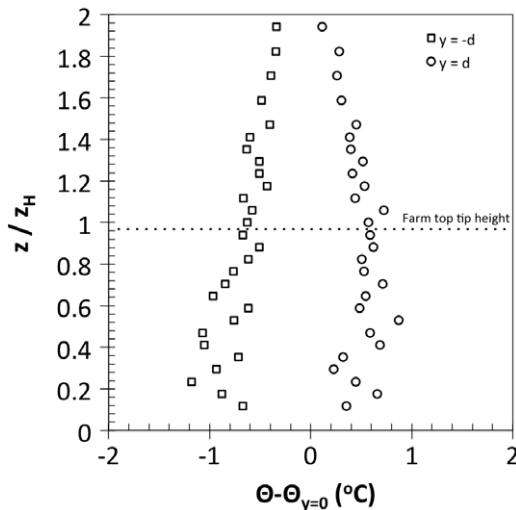
Figure 8. Vertical profiles of the difference in mean temperature at $y/d = -1$ and 1 compared to at $y/d = 0$ in the aligned wind farm.

wind-turbine column at $y/d = -1$ and 1 compared to the profile measured at the centerline, $y/d = 0$, shows a behavior that supports this argument (see figure 8). Compared to what happens in the aligned wind farm, multiple wakes mix much more efficiently in the staggered wind farm, resulting in a relatively uniform distribution of the surface heat flux.

5. Summary and conclusions

Wind-tunnel experiments were conducted to examine the effects of a large-scale wind farm with typical layout on the spatial distribution and net change of the surface heat flux, in a turbulent boundary layer with a surface heat source. For the case of a staggered wind farm, except for an increase in the near-wake region of the turbine, the surface heat flux exhibits a relatively uniform distribution and an overall reduction of approximately 4% with respect to the boundary-layer flow without wind turbines. In the aligned farm, two distinctive regions of increased and decreased surface heat flux on either side of turbine columns were identified. The decreased flux on the upwelling side has a similar magnitude as the increased flux on the downwelling side, resulting in a nearly zero net change in the overall surface heat flux. However, the difference between the minimum and maximum surface heat flux is about 12% and 7% in the aligned and staggered wind farm, respectively.

Vertical profiles of near-surface temperature, kinematic heat flux and heat transport efficiency, measured in the quasi-developed flow regime, show evidence supportive of the surface heat flux change in the staggered wind farm. It is found that the turbulent momentum and heat transport near the surface is very different from that above the wind farm; higher turbulence and increased heat flux above does not necessarily translate to higher surface heat flux in a wind farm. In addition, a 1D energy balance is presented to explain the surface heat flux change in terms of internal energy change in the flow due to the presence of a wind farm.

This work provides the first direct measurements of surface heat flux distribution in well-controlled conditions. Though the overall surface heat flux change induced by wind farms is small, the highly heterogeneous spatial distribution of the surface heat flux, dependent on the wind-farm layouts, is significant. These findings are important, in particular when considering colocation of wind farms with intensive agriculture practice, as the change in surface heat flux due to wind farms may affect irrigation requirement and crop yields. Future experiments are planned to conduct similar measurements with varying wind-turbine distribution and configuration under different thermal stratification conditions.

Additionally, attribution of the well-marked surface heat flux distribution to the coherent rotating wake column in the aligned farm suggests that it is essential to simulate the wake rotation effects in numerical models of wind-farm flows in order to reproduce the spatial distribution of the surface heat flux. Without simulating the wake rotation effects, turbulent mixing might be underestimated in the wake, resulting in incorrectly simulated momentum and heat transport near the surface. Parameterization of wind turbines using the actuator line model (ALM) and actuator disk with rotation model (AMD-R) in LES studies by Porté-Agel *et al* (2011) and Wu and Porté-Agel (2011) has demonstrated promising capability to reproduce important turbulent wake features in wind farms, such as the helicoidal tip vortices, enhanced turbulence level near the top-tip height and wake rotation. Further investigation of surface fluxes within large wind farms using our LES framework is planned for different wind-farm layouts and turbine spacing.

References

Baidya Roy S 2011 Simulating impacts of wind farms on local hydrometeorology *J. Wind Eng. Indust. Aerodyn.* **99** 491–8

Baidya Roy S, Pacala S W and Walko R L 2004 Can large wind farms affect local meteorology? *J. Geophys. Res.* **109** 1–6

Baidya Roy S and Traiteur J J 2010 Impacts of wind farms on surface air temperatures *Proc. Natl Acad. Sci.* **107** 17899–904

Barrie D B and Kirk-Davidoff D B 2010 Weather response to a large wind turbine array *Atmos. Chem. Phys.* **10** 769–75

Cal R B, Lebrón J, Castillo L, Kang H S and Meneveau C 2010 Experimental study of the horizontally averaged flow structure

in a model wind-turbine array boundary layer *J. Renew. Sustain. Energy* **2** 013106

Calaf M, Meneveau C and Meyers J 2010 Large eddy simulation study of fully developed wind-turbine array boundary layers *Phys. Fluids* **22** 015110

Calaf M, Parlange M and Meneveau C 2011 Large eddy simulation study of scalar transport in fully developed wind-turbine array boundary layers *Phys. Fluids* **23** 126603

Chamorro L P, Arndt R E A and Sotiropoulos F 2011 Turbulent flow properties around a staggered wind farm *Bound.-Layer Meteorol.* **141** 349–67

Chamorro L P and Porté-Agel F 2011 Turbulent flow inside and above a wind farm: a wind-tunnel study *Energies* **11** 1916–36

Fitch A C, Olson J B, Lundquist J K, Dudhia J, Gupta A K, Michalakes J and Barstad I 2012 Local and mesoscale impacts of wind farms as parameterized in a mesoscale NWP model *Mon. Weather Rev.* **140** 3017–38

Frandsen S, Barthelmie R, Pryor S, Rathmann O, Larsen S, Højstrup J and Thøgersen M 2006 Analytical modelling of wind speed deficit in large offshore wind farms *Wind Energy* **9** 39–53

Frandsen S T, Jørgensen H E, Barthelmie R, Rathmann O, Badger J, Hansen K, Ott S, Rethore P E, Larsen S E and Jensen L E 2009 The making of a second-generation wind farm efficiency model complex *Wind Energy* **12** 445–58

Gunturu U B and Schlosser C A 2012 Characterization of wind power resource in the United States *Atmos. Chem. Phys.* **12** 9687–702

Ivanova L A and Nadyozhina E D 2000 Numerical simulation of wind farm influence on wind flow *Wind Energy* **24** 257–69

Keith D W, DeCarolis J F, Denkenberger D C, Lenschow D H, Malyshev S L, Pacala S and Rasch P J 2004 The influence of large-scale wind power on global climate *Proc. Natl Acad. Sci.* **101** 16115–20

Lu H and Porté-Agel F 2011 Large-eddy simulation of a very large wind farm in a stable atmospheric boundary layer *Phys. Fluids* **23** 065101

Markfort C M, Zhang W and Porté-Agel F 2012 Turbulent flow and scalar flux through and over aligned and staggered wind farms *J. Turbul.* **13** N33

Meneveau C 2012 The top–down model of wind farm boundary layers and its applications *J. Turbul.* **13** N7

Porté-Agel F, Lu H, Wu Y T and Conzemius R J 2011 Large-eddy simulation of atmospheric boundary layer flow through wind turbines and wind farms *J. Wind Eng. Indust. Aerodyn.* **99** 154–68

Rajewski D A, Takle E S, Lundquist J K, Oncley S P, Prueger J H, Horst T W, Rhodes M E, Pfeiffer R, Hatfield J L, Spoth K K and Doorenbos R K 2012 CWEX: Crop/Wind-1 energy EXperiment: observations of surface-layer, boundary-layer and mesoscale interactions with a wind farm *Bull. Am. Meteorol. Soc.* at press (doi:10.1175/BAMS-D-11-00240)

Roth M and Oke T R 1995 Relative efficiencies of turbulent transfer of heat, mass and momentum over a patchy urban surface *J. Atmos. Sci.* **52** 1863–74

Vermeer L J, Sørensen J N and Crespo A 2003 Wind turbine wake aerodynamics *Prog. Aerospace Sci.* **39** 467–510

Wang C and Prinn R G 2010 Potential climatic impacts and reliability of very large-scale wind farms *Atmos. Chem. Phys.* **10** 2053–61

Wang C and Prinn R G 2011 Potential climatic impacts and reliability of large-scale offshore wind farms *Environ. Res. Lett.* **6** 025101

Wu Y T and Porté-Agel F 2011 Large-eddy simulation of wind-turbine wakes: evaluation of turbine parametrisations *Bound.-Layer Meteorol.* **138** 345–66

Wu Y T and Porté-Agel F 2012 Simulation of turbulent flow inside and above wind farms: model validation and layout effects *Bound.-Layer Meteorol.* at press (doi:10.1007/s10546-012-9757-y)

Zhang W, Markfort C M and Porté-Agel F 2012a Near-wake flow structure downwind of a wind turbine in a turbulent boundary layer *Exp. Fluids* **52** 1219–35

Zhang W, Markfort C M and Porté-Agel F 2012b Wind-turbine wakes in a convective boundary layer: a wind-tunnel study *Bound.-Layer Meteorol.* at press (doi:10.1007/s10546-012-9751-4)

Zhou L M, Tian Y H, Baidya Roy S, Thorncroft C, Bosart L F and Hu Y L 2012 Impacts of wind farms on land surface temperature *Nature Clim. Change* **2** 539–43